

Transport of Pacific Water into the Canada Basin

Michael A. Spall¹, Robert S. Pickart¹, Min Li^{1,2,3,4}, Motoyo Itoh⁵, Peigen Lin¹,
Takashi Kikuchi⁵, Yiquan Qi⁶

¹Woods Hole Oceanographic Institution, Woods Hole, MA 02543

²State Key Laboratory of Tropical Oceanography, South China Sea Institute of Oceanology, Chinese

Academy of Sciences, Guangzhou, Guangdong 510301, China

³Guangdong Province Key Laboratory for Coastal Ocean Variation and Disaster Prediction, Guangdong

Ocean University, Zhanjiang, Guangdong 524088, China

⁴University of Chinese Academy of Sciences, Beijing 100049, China

⁵Japan Agency for Marine-Earth Science and Technology, Yokosuka, Kanagawa, Japan

⁶College of Oceanography, Hohai University, Nanjing, Jiangsu 210098, China

Key Points:

- Westward flow of Pacific origin waters is observed off the shelfbreak north of the Chukchi Sea
- A regional numerical model traces these waters to the outflow of Barrow Canyon
- This nonlinear advection dominates the cross-isobath flow and supply of Pacific origin waters to the Canada Basin

Abstract

A high resolution regional ocean model together with moored hydrographic and velocity measurements are used to identify the pathways and mechanisms by which Pacific Water, modified over the Chukchi shelf, crosses the shelfbreak into the Canada Basin. Most of the Pacific Water flowing into the Arctic Ocean through Bering Strait enters the Canada Basin through Barrow Canyon. Strong advection allows the water to cross the shelfbreak and exit the shelf. Wind forcing plays little role in this process. Some of the outflowing water from Barrow Canyon flows to the east into the Beaufort Sea, however, approximately 0.4 to 0.5 Sv turns to the west forming the newly identified Chukchi Slope Current. This transport occurs at all times of year, channeling both summer and winter waters from the shelf to the Canada Basin. The model indicates that approximately 75% of this water was exposed to the mixed layer within the Chukchi Sea, while the remaining 25% was able to cross the shelf during the stratified summer before convection commences in late fall. We view the $\mathcal{O}(0.5)$ Sv of the Chukchi Slope Current as replacing Beaufort Gyre water that would have come from the east in the absence of the cross-topography flow in Barrow Canyon. The eastward flow on the Beaufort slope is also consistent with the local disruption of the Beaufort Gyre by the Barrow Canyon outflow.

1 Introduction

Pacific-origin water strongly influences the hydrographic structure of the western Arctic Ocean and plays a critical role in the functioning of the regional ecosystem. The upper halocline of the Canada Basin contains warm Pacific summer water atop cold Pacific winter water, which together dictate the stratification that shields the underlying warm Atlantic layer from the pack ice. The cold Pacific water also supplies the basin with nutrients [Codispoti *et al.*, 2005] as well as carbon [Mathis *et al.*, 2007], the latter of which is now contributing to enhanced levels of ocean acidification [Cross *et al.*, 2017]. Zooplankton and other organisms are fluxed into the Canada Basin with the warm Pacific water [Ashjian *et al.*, 2010; Nelson *et al.*, 2009; Hopcroft *et al.*, 2010], which in turn influence the feeding patterns of upper trophic species [Wassmann *et al.*, 2015]. The warmest summer water also represents a significant source of freshwater to the western Arctic [Woodgate *et al.*, 2012] which is accumulated in the Beaufort Gyre [Proshutinsky *et al.*, 2009]. Despite these and other known impacts of Pacific water, there remains considerable uncertainty as to how and where the water is transported from the shelves into the interior. A better understanding of this shelf-basin transfer of mass and properties is thus required, not only to enhance our knowledge of the western Arctic ecosystem, but to be able to predict how it might change in response to a warming climate.

Over the years a number of observational and modeling studies have sharpened our view of the circulation and modification of Pacific water as it progresses across the Chukchi shelf. To first order, there are three main flow branches, largely dictated by the topography of the shelf: the coastal branch (known in summertime as the Alaskan Coastal Current, e.g. Paquette and Bourke [1974]), the Central Channel branch [e.g. Weingartner *et al.*, 2005], and the western branch that flows through Herald Canyon [Woodgate *et al.*, 2005a; Pickart *et al.*, 2010, see Fig. 1]. Numerical models generally support this view, although they indicate that the shelf circulation is highly sensitive to synoptic wind forcing [Winsor and Chapman, 2004; Spall, 2007; Panteleev *et al.*, 2010]. For example, the flow in all three branches can be reversed to the south under northerly winds [Weingartner *et al.*, 2017; Pickart *et al.*, 2010, 2011], as can the flow through Bering Strait [Woodgate *et al.*, 2005b]. Recently, it has been demonstrated that these flow branches interact with each other to some degree. For example, part of the western branch north of Herald Canyon is diverted to the central branch, which subsequently splits into smaller filaments that converge with the coastal branch as the water enters Barrow Canyon (see Fig. 1).

68 Despite our improving understanding of the circulation of the Chukchi Sea, the man-
 69 ner and location in which the Pacific water subsequently exits the shelf into the basin
 70 is still far from clear. This is complicated by the topography of the Chukchi Sea, in which
 71 the definition of what is the shelf and what is the basin interior is ambiguous. For ex-
 72 ample, the depth at which the shelfbreak occurs varies by as much as 100 m (B. Cor-
 73 lett, pers. comm., 2017). Using sparsely positioned moorings spanning the Chukchi Sea,
 74 *Woodgate et al.* [2005a] argued that, averaged over the year, roughly equal amounts of
 75 Pacific water leave the shelf through Long Strait, Herald Canyon, and Barrow Canyon.
 76 If or where these waters enter the basin (versus remaining on the outer shelf) is not known.
 77 During the summer months it appears that the majority of the Pacific water can at times
 78 flow through Barrow Canyon [*Itoh et al.*, 2013; *Gong and Pickart*, 2015; *Pickart et al.*,
 79 2016]. Part of the uncertainty is due to the fact that, to date, there have been no high-
 80 resolution mooring arrays deployed in Long Strait or Herald Canyon, hence we have no
 81 robust observational estimates of the transport through these geographical constrictions.
 82 Moreover, the mooring arrays deployed within and near Barrow Canyon have provided
 83 differing results. For example, *Itoh et al.* [2013] report a yearly mean Pacific water trans-
 84 port of 0.44 Sv at the mouth of the canyon, while *Weingartner et al.* [2017] estimate a
 85 mean value of only 0.20 Sv at the head of the canyon. This discrepancy could be due in
 86 part to instrument coverage. The climatological transport through Bering Strait is of
 87 $O(0.8 \text{ Sv})$ [*Woodgate et al.*, 2005b], although this has recently increased to an annual mean
 88 value of 1.1 Sv [*Woodgate*, 2017].

89 It is possible that there is a net flux of Pacific water across the Chukchi shelfbreak
 90 due to turbulent or wind-driven processes. It is now well established that, in the absence
 91 of wind, there is an eastward-flowing current along the shelfbreak of the Chukchi Sea [*Cor-*
 92 *lett and Pickart*, 2017; *Watanabe et al.*, 2017; *Li et al.*, submitted]. The jet is baroclin-
 93 ically unstable and can spawn both cold-core and warm-core eddies of Pacific water [*Pickart*
 94 *et al.*, 2005; *Pickart and Stossmeister*, 2009; *Mathis et al.*, 2007]. We note the numer-
 95 ical model study of *Spall et al.* [2008] suggests that, while this process fluxes tracers off-
 96 shore, there is no net mass flux, i.e. it is an exchange of water. On the other hand, *Tim-*
 97 *mermans et al.* [2017] argue that Pacific water is subducted from the mixed layer on the
 98 Chukchi shelf to the halocline of the Canada Basin by wind forcing via a combination
 99 of lateral induction and Ekman pumping. Using a numerical model they estimate that
 100 this results in net flux of 0.4 Sv across the Chukchi shelfbreak, which is the same mag-
 101 nitude that *Itoh et al.* [2013] estimate flows out of Barrow Canyon.

102 Recently, *Corlett and Pickart* [2017] have documented the existence of a westward-
 103 flowing current along the continental slope of the Chukchi Sea – seaward of the shelf-
 104 break jet – which they named the Chukchi Slope Current. Using 46 shipboard crossings
 105 of the current occupied over a period of 12 years, *Corlett and Pickart* [2017] estimate
 106 that it transports 0.5 Sv of Pacific water. They argue that the $O(50 \text{ km})$ wide slope cur-
 107 rent emanates from the outflow from Barrow Canyon, which is consistent with the ship-
 108 board measurements discussed in *Brugler et al.* [2014] and the surface drifter trajecto-
 109 ries presented in *Weingartner et al.* [2015] and *Stabeno et al.* [2018]. While the shipboard
 110 data used by *Corlett and Pickart* [2017] were collected exclusively during the summer
 111 months, a mooring array deployed west of Barrow Canyon has confirmed that the Chukchi
 112 Slope Current is a year-round feature [*Li et al.*, submitted]. Averaged over the year, the
 113 current is surface intensified.

114 In summer the current is surface intensified, and during the cold months of the year
 115 it is middepth-intensified. This latter observation is consistent with the modeling results
 116 of *Watanabe et al.* [2017]. By taking into account the Chukchi Slope Current, *Corlett*
 117 *and Pickart* [2017] were able to construct a balanced mass budget of the inflows/outflows
 118 of the Chukchi shelf. This seems to be at odds with the large off-shelf subduction of Pa-
 119 cific water that *Timmermans et al.* [2017] calculate. It should be noted, however, that
 120 the model employed by *Timmermans et al.* [2017] is coarse (36 km lateral resolution)

and thus incapable of resolving either the Chukchi shelfbreak jet or the Chukchi Slope Current.

In the interior Canada Basin the circulation is dominated by the Beaufort Gyre, which is driven by the anti-cyclonic wind stress curl associated with the Beaufort High [Moore, 2012]. The gyre varies in size and strength on seasonal timescales [Proshutinsky *et al.*, 2002] as well as interannually [Proshutinsky *et al.*, 2009]. Over the past decade the freshwater content of the gyre has significantly increased due to an extended period of anticyclonic atmospheric forcing [Proshutinsky *et al.*, 2015]. Using satellite measurements of sea surface height, Mizobata *et al.* [2016] demonstrated that the gyre varies from month to month, yet the surface speeds of the gyre generally remain on the order of 10 cm/s. Using their calculated velocity fields, Mizobata *et al.* [2016] investigated the fate of Pacific water in the Canada Basin by releasing a passive tracer in the vicinity of Barrow Canyon for different years. The tracer was consistently advected to the west and then north by the gyre, although in some years much of it remained close to the shelfbreak of the Chukchi and East Siberian Seas. However, no mention was made of a slope current over the continental slope. Watanabe *et al.* [2017] did a similar tracer release in their model and also found that a large proportion of the Pacific water emanating from Barrow traveled to the west. They noted that this pathway was distinct from the southern arm of the Beaufort Gyre and referred to it as a shelfbreak flow. Considering the observations of Corlett and Pickart [2017] and Li *et al.* [submitted], it is clear that the Watanabe *et al.* [2017] westward pathway is the Chukchi Slope Current. A similar anticyclonic circulation was found for water originating on the shelf in a model by Timmermans *et al.* [2014], although the resolution of the model was likely not sufficient to distinguish the Chukchi Slope Current from the Beaufort Gyre.

In light of these recent studies, numerous questions arise regarding the circulation north of the Chukchi Sea and the fate of the Pacific water emanating from the shelf. For instance, does a sizable portion of the outflow from Barrow Canyon turn west to form the Chukchi Slope Current? If so, what are the dynamics that govern this? Also, what is the fate of the Pacific water advected by the current and how does it enter the basin? What are the relative contributions to the source waters of the Canada Basin halocline from the advective outflow from Barrow Canyon versus subduction from the mixed layer of the Chukchi Sea across the shelfbreak to the west of Barrow Canyon? Finally, how is the Chukchi Slope Current related to the southern portion of the Beaufort Gyre? In this study we address some of these questions.

2 Methods

A regional numerical model and mooring observations are used to describe the circulation in the vicinity of the Chukchi shelfbreak, Barrow Canyon, and the southern Beaufort Gyre. The observations are used to identify the currents, document transports, and infer pathways based on water mass properties. The numerical model is first evaluated in terms of its ability to reproduce the basic characteristics of the flow observed at key locations, and then used to identify the pathways and mechanisms of exchange across the Chukchi shelfbreak.

2.1 Observational resources

Timeseries from three different mooring arrays are used in the study: a high-resolution array that was deployed across the Beaufort Sea shelf/slope; three moorings that have been maintained across the mouth of Barrow Canyon; and an array that spanned from the outer shelf to the upper slope of the Chukchi Sea. These are shown in Fig. 2. The Beaufort array was part of the Western Arctic Shelf-Basin Interactions (SBI) program and was in place from August 2002 to September 2004. This consisted of seven moorings spanning from the outer shelf to the mid continental slope. The inner five moor-

171 ings contained coastal moored profilers providing vertical traces of temperature and salin-
 172 ity four times daily at 2-meter resolution. The profiles extended only to 50m depth, since
 173 it was deemed unsafe to have the mooring top floats be any shallower than this due to
 174 the risk of ridging pack ice. Velocity at these sites was measured using upward-facing
 175 acoustic Doppler current profilers (ADCPs) near the bases of the moorings. These pro-
 176 vided vertical traces of eastward and northward currents at 5-10 m resolution every hour.
 177 The two offshore moorings contained McLane moored profilers sampling twice per day.
 178 The velocity at these sites was measured by a travel time acoustic current meter on the
 179 profiler. The resolution of both the hydrographic and velocity profiles was 2 m. The ve-
 180 locity data from all of the moorings were de-tided using the T-TIDE harmonic analy-
 181 sis toolbox (Pawlowicz et al., 2002). The reader is referred to *Spall et al.* [2008], *Nikolopou-*
 182 *los et al.* [2009], and *Li and Pickart* [2017] for details regarding the processing of the moor-
 183 ing data and the accuracy of the measurements.

184 More recently, a single mooring near the shelfbreak (mooring BS3, Fig. 2) has been
 185 maintained since 2008 as part of the Arctic Observing Network (AON). This was con-
 186 figured similarly to the original mooring at the site, but in recent years the profiler has
 187 been replaced by discrete MicroCATs. Also, in some years two ADCPs have been used,
 188 one near the bottom and a second upward-facing instrument on the top float. Further
 189 details regarding the AON mooring can be found in Brugler et al. (2014) and Lin et al.,
 190 (2018). The transport of boundary current is estimated for these years using a proxy that
 191 was developed by Brugler et al. (2014) and shown to be highly accurate.

192 The moorings in Barrow Canyon are maintained by the Japan Agency for Marine-
 193 Earth Science and Technology (JAMSTEC), and have been in place (with some inter-
 194 ruptions) since 1999. The moorings are spaced 10 km apart and contain MicroCATs for
 195 measuring pressure, temperature, and salinity, and a combination of point current met-
 196 ers and ADCPs for velocity. The upper-most MicroCATs are situated near 30 m depth.
 197 The data are interpolated onto a regular grid and low-passed using a 25-hour filter width.
 198 *Itoh et al.* [2013] provide details the data configuration, processing, and accuracy of the
 199 sensors.

200 The mooring array spanning the Chukchi shelfbreak and upper-slope was deployed
 201 as part of a program entitled “Characterization of the Circulation on the Continental
 202 Shelf Areas of the Northeast Chukchi and Western Beaufort Seas”. The array was com-
 203 prised of five moorings deployed from October 2013 to September 2014. Each of the moor-
 204 ings contained a coastal moored profiler providing vertical traces of temperature and salin-
 205 ity at 2-m resolution four times per day, and an upward-facing ADCP providing hourly
 206 vertical profiles of velocity. The top floats of the moorings were situated at 35 m depth.
 207 All of the velocity data were de-tided in the same way as for the Beaufort slope moor-
 208 ing data. Details concerning the instrumentation and the data are given in *Li et al.* [sub-
 209 mitted]. At all of the array sites we defined Pacific water as fresher than 34, following
 210 *Itoh et al.* [2013]. We also use climatological data from the Bering Strait mooring array
 211 published in *Woodgate et al.* [2005b].

212 2.2 Model configuration and forcing

213 A regional version of the Massachusetts Institute of Technology general circulation
 214 model (MITgcm), *Marshall et al.* [1997], is set up for the Chukchi Sea and Canada Basin.
 215 It solves the hydrostatic, primitive equations of motion on a staggered Cartesian C-grid
 216 at fixed depth levels. The partial cell treatment of bottom topography allows for accu-
 217 rate representation of steep topography in the presence of stratification, expected to be
 218 important for the exchange of properties across the shelfbreak.

219 The model is coupled to a thermodynamic/dynamic sea ice model. (Details can be
 220 found at http://mitgcm.org/public/r2_manual/latest/online_documents/node2.html.) The
 221 dynamics are elastic-viscous-plastic [*Hunke and Dukowicz*, 1997]. The thermodynam-

222 ics are modeled with a three layer scheme that permits heat storage in ice [*Semtner, 1976*],
 223 as reformulated by *Winton* [2000]. The albedo reflects that of wet (0.66) or dry (0.75)
 224 ice, depending on if there is sufficient heat flux to form melt ponds. The model repre-
 225 sents two layers of ice (the upper layer has variable heat capacity resulting from brine
 226 pockets) and an overlying layer of snow. The model produces ice thickness and concen-
 227 tration.

228 The domain is set on an f -plane with the Coriolis parameter constant at $f_0 =$
 229 $1.2 \times 10^{-4} \text{ s}^{-1}$. The model is configured on a 1465 km by 2158 km Cartesian grid with
 230 the southwest corner at 63° N and 180° W . The western boundary of the model domain
 231 follows the 180° meridian while the southern boundary follows the 63° N latitude cir-
 232 cle. The grid spacing is variable, ranging from 2 km in the vicinity of Barrow Canyon
 233 to 5 km over the Chukchi Sea and southern Canada Basin, to 11 km on the offshore side
 234 of the Beaufort Gyre (Fig. 3). The bottom topography is interpolated from the ETOPOv2
 235 global topography on a 2 minute grid to the model grid. The maximum depth in the model
 236 is 1000 m. The vertical grid spacing is 5 m over the upper 80 m depth, gradually increas-
 237 ing to 50 m at 250 m depth and further increasing to 200 m between 800 m and 1000
 238 m. There is also a channel connecting the eastern shelf with the inflow at Bering Strait.
 239 A similar configuration of the model was used by *Spall* [2007] in a lower resolution study
 240 of the circulation in the Chukchi Sea.

241 Subgridscale horizontal viscosity A is parameterized by the *Smagorinsky* [1963] deformation-
 242 dependent scheme as

$$A = \left(\frac{\nu\delta}{\pi}\right)^2 D, \quad D = [(u_x - v_y)^2 + (u_y + v_x)^2]^{1/2} \quad (1)$$

243 where δ is the model grid spacing, $\nu = 2.5$ is a nondimensional coefficient, D is the de-
 244 formation field, and subscripts indicate partial differentiation. Vertical viscosity and dif-
 245 fusivity are represented with the KPP mixing parameterization [*Large et al., 1994*] and
 246 background mixing coefficients of $10^{-5} \text{ m}^2 \text{ s}^{-1}$. There is also a quadratic bottom drag
 247 with coefficient 2×10^{-3} . The lateral boundary conditions are no-slip and no normal
 248 flux. The model utilizes the nonlinear equation of state of *Jackett and McDougall* [1995].

249 The model is initialized with temperature and salinity interpolated from the PHC3.0
 250 January climatology, updated from *Steele et al.* [2001]. North of $y = 1250 \text{ km}$ and at
 251 depths below 35 m the temperature and salinity in the model are restored towards this
 252 climatology with a time scale of $2.5 \times 10^6 \text{ s}$. This helps to maintain the anticyclonic Beau-
 253 fort Gyre circulation in the presence of the model solid boundaries in the basin interior.
 254 The fields in the Chukchi Sea, in the vicinity of Barrow Canyon and the shelfbreak, and
 255 in the seasonal mixed layer in the Beaufort Gyre, are freely evolving; there are no ar-
 256 tificial restoring terms.

257 The model is forced by surface fluxes of heat, fresh water, and momentum derived
 258 from the monthly mean North American Regional Reanalysis model output (32 km grid,
 259 averaged between years 1979 and 2000, <http://www.esrl.noaa.gov/psd/data/gridded/data.narr.html>).
 260 The sensible and latent heat fluxes are derived from 10 m atmospheric winds, 2 m at-
 261 mospheric temperature, and specific humidity using the bulk formulae of *Large and Pond*
 262 [1981]. The downward longwave and shortwave radiation are also specified, while the out-
 263 going longwave radiation is calculated from the surface temperature. The surface mo-
 264 mentum flux is derived from atmospheric winds.

265 The model is also forced by transport through Bering Strait. The volume flux, tem-
 266 perature, and salinity of the inflowing water are based on long-term measurements in the
 267 strait [*Woodgate et al., 2005b; Weingartner et al., 2005*], as in *Spall* [2007]. This is achieved
 268 by strongly restoring the model temperature, salinity, and meridional velocity towards
 269 prescribed values within the gray box in Bering Strait in Fig. 3. The hydrographic prop-

270 erities and transport of the inflow vary with season, with cold, salty water in winter and
 271 warm, fresh water in summer and fall.

272 The central model was run for two years with repeat monthly mean atmospheric
 273 forcing. Several sensitivity calculations were also carried out. In one, the Bering Strait
 274 is closed and all other forcing is the same as the central case, while in another calculation
 275 the forcing in Bering Strait is the same but all atmospheric forcing and sea ice are
 276 eliminated. This pair of calculations is used to help understand the forcing mechanism
 277 for the Chukchi Slope Current and to distinguish it from the Beaufort Gyre. A final calculation
 278 in which all forcing was the same except the velocity towards which the model
 279 is restored in Bering Strait and the winds were set to the annual mean (no seasonal cycle)
 280 is used to demonstrate that the seasonal cycle in Chukchi Slope Current transport
 281 is related to the seasonal cycle in stratification, not transport in Bering Strait.

282 3 Mean circulation

283 The mean model transport streamfunction in the upper 300 m is shown in Fig. 4
 284 along with the bottom topography. The mean transport through Bering Strait is 0.81
 285 Sv, consistent with the long-term measurements of *Woodgate et al.* [2005b]. The flow over
 286 the Chukchi shelf is in line with observational estimates [*Woodgate et al.*, 2005a] and the
 287 previous model of *Spall* [2007]. In particular, there are three primary pathways: through
 288 Herald Canyon, through the Central Channel, and along the Alaskan coast. Most of this
 289 transport follows the topography and turns towards the east along the outer shelf, con-
 290 verging at the head of Barrow Canyon. Due to the convergence of topographic contours,
 291 there is very rapid flow through the canyon.

292 At the mouth of Barrow Canyon most of the Pacific water flows across the shelf-
 293 break and enters the basin interior. Roughly 0.4 Sv turns towards the west, and about
 294 0.2 Sv turns towards the east (about 0.2 Sv remains on the shelf and flows towards the
 295 east). This result supports the argument made by *Corlett and Pickart* [2017] that the
 296 westward-flowing Chukchi Slope Current emanates from Barrow Canyon. It is also con-
 297 sistent with surface drifter studies [*Weingartner et al.*, 2015; *Stabeno et al.*, 2018] as well
 298 as with the numerical results of *Watanbe et al.* (2017) who focused on the circulation
 299 during the winter months. To the north of the Chukchi Sea, the Beaufort Gyre spans
 300 most of the deep basin in the model, with a transport of just over 1 Sv. Note that this
 301 circulation and hydrography for y greater than 1250 km is largely constrained by the PHC3.0
 302 climatology to which the model hydrography is restored. The shape of the model Beau-
 303 fort Gyre looks different from the usual polar projection but is consistent with this cli-
 304 matological hydrography. South of this restoring region, and east of Barrow Canyon (within
 305 about 200 km of the north slope of Alaska) there is a weak, meandering flow towards the
 306 east, transporting water that originated from Barrow Canyon. This fluid, plus that which
 307 turned west at Barrow Canyon, ultimately closes the circulation to the south in the chan-
 308 nel along the eastern boundary, to be returned to the Chukchi Sea through Bering Strait.

309 Our focus is on the sources of Pacific water that cross the shelfbreak at Barrow Canyon
 310 and turn westward. However, before addressing this we first discuss the flow through the
 311 canyon and the portion of it that turns to the east on the shelf, as these components of
 312 the circulation are reasonably well established in the observational literature. The mean
 313 velocity and salinity in the model within Barrow Canyon (the western bold red line in
 314 Fig. 4) are shown in Fig. 5a. The flow through the canyon has a mid-depth maximum
 315 and is banked up against the southeastern side. The maximum zonal velocity is about
 316 22 cm s^{-1} . The water is weakly stratified at mid-depth over the eastern flank of the canyon.
 317 The climatological mean along-canyon velocity measured by the JAMSTEC array is also
 318 characterized by a mid-depth maximum (roughly 17 cm s^{-1}), with the strongest flow on
 319 the eastern flank of the canyon (Fig. 5b). As is the case in the model, the eastern flank

320 has weaker stratification than offshore (recall that the mooring data does not extend above
321 30 m depth).

322 To the east of Barrow Canyon, the mean zonal velocity in the model (the eastern
323 bold red line in Fig. 4) is shown in Fig. 6a. The zonal flow has a subsurface maximum
324 of about 8 cm s^{-1} centered just off the shelfbreak. The mean current is fairly narrow,
325 about 20 km wide, and is concentrated in the upper 200 m. The water in the current
326 has weaker stratification (low potential vorticity) as a result of convectively formed win-
327 ter water originating on the Chukchi shelf (e.g. Pickart et al., 2005). Such a mean kine-
328 matic and water mass structure of the Beaufort shelfbreak jet is in line with the obser-
329 vations in Fig. 6b (Nikolopoulos et al., 2009), although the observed current is much nar-
330 rower and faster than that in the model (note that the salinity data from the moorings
331 is limited to depths deeper than 50 m).

332 4 Flux of Pacific origin water across the shelfbreak

333 As seen above, the regional model produces currents and transports through the
334 Chukchi Sea, Barrow Canyon, and along the shelfbreak east of Barrow that are consis-
335 tent with the observations. We now use the model fields to connect the westward flow
336 seaward of the Chukchi shelfbreak to the Chukchi Slope Current and the northward trans-
337 port through Barrow Canyon. For purposes of discussion, we define Chukchi shelf to ex-
338 tend to the 100 m isobath and the upper slope to lie between the 100 m isobath and the
339 300 m isobath. Offshore of the 300 m isobath we refer to as the Canada basin interior.

340 *Chukchi Slope Current*

341 The 46 shipboard sections used by *Corlett and Pickart* [2017] indicated that the
342 Chukchi Slope Current transports 0.50 Sv of Pacific origin waters towards the west dur-
343 ing the summer months, offshore of the shelfbreak. Using data from the mooring array
344 across the Chukchi shelfbreak/upper-slope (Fig. 2), *Li et al.* [submitted] estimated a sim-
345 ilar value (0.57 Sv) for the annual mean transport. (The mooring array did not capture
346 the offshore edge of the current, so *Li et al.* [submitted] applied an extrapolation tech-
347 nique. Nevertheless, it is likely that their mean transport value is an underestimate.) The
348 presence of Pacific water in the upper halocline of the Canada Basin is well established
349 (e.g. Steele et al., 2004). There have been several mechanisms proposed as a means to
350 transport the Pacific water across the shelfbreak. Instabilities of the shelfbreak jet pro-
351 duce small eddies with modified Pacific water in their core [*Pickart et al.*, 2005; *Mathis*
352 *et al.*, 2007]. While commonly observed in the basin interior [*Manley and Hunkins*, 1985;
353 *Zhao et al.*, 2014], these are distinct from the large-scale westward flow of the Chukchi
354 Slope Current. Previous models of the region have produced an offshore flow from Bar-
355 row Canyon into the basin interior [*Zhang et al.*, 2016; *Aksenov et al.*, 2016], but these
356 models had lower spatial resolution and did not focus on this shelf-basin exchange. The
357 recent study by *Watanabe et al.* [2017] used observations and a high resolution Arctic
358 model to connect a seasonal warming of the halocline in the Chukchi Borderland region
359 to outflow from Barrow Canyon via westward advection by the slope current (which they
360 referred to as a shelfbreak flow).

361 The model velocity parallel to the 75 m isobath, averaged over the final 6 months
362 of integration along the shelf between $x = 600 \text{ km}$ and $x = 830 \text{ km}$, is shown as a func-
363 tion of offshore distance and depth in Fig. 7a. We chose the final 6 months in order to
364 show the penetration of a tracer marking Pacific origin water (Fig. 7c), and the along-
365 shelf average to avoid aliasing meanders and eddies that are present at any particular
366 section. There is a bottom intensified eastward flow centered near the shelfbreak ($0 <$
367 $x < 30 \text{ km}$) and a surface intensified westward flow just offshore of the shelfbreak ($30 <$
368 $x < 150 \text{ km}$). These correspond with the Chukchi shelfbreak jet and Chukchi Slope Cur-
369 rent, respectively. The westward flow at the offshore part of the section ($150 < x <$

200 km) is the southern arm of the Beaufort Gyre (see below). The model Chukchi Slope Current is salt stratified while the shelfbreak jet (which emanates from Herald Canyon) has a weakly stratified core (Fig. 7c), indicating low potential vorticity as a result of wintertime convection in the Chukchi Sea. This compares favorably to the summertime mean slope current section of *Corlett and Pickart* [2017] as well as the year-long mean section of *Li et al.* [submitted] constructed using the mooring data (Fig. 7b), although the model current is slower and wider than the observations. As noted above, Li et al's (submitted) section does not bracket the entire slope current, but Corlett and Pickart's (2017) section does extend seaward of the current and captures the southern edge of the westward-flowing Beaufort Gyre.

Mean shelf-basin flux

The mean transport perpendicular to the 100 m isobath (see Fig. 3 for reference) indicates where the Pacific water exits the shelf. The mean transport over the two year integration was calculated relative to the western boundary in the model and integrated downward from the surface along the 100 m isobath (Fig. 8). Regions of vertical gradients indicate the depths, and horizontal gradients indicate the along-shelf location, of the flow across the topography. The primary region of exchange is at a distance 1300 km from the western boundary, the location of Barrow Canyon. It occurs throughout the water column but is most concentrated between 50m and 80 m depth. This is consistent with the subsurface maximum in the mean velocity in Barrow Canyon. There is a net flux across the 100 m isobath west of Barrow Canyon of about 0.2 Sv. This occurs primarily along the steep slope between $x = 800$ km and the western flank of Barrow Canyon. The offshore flux is concentrated near the bottom, suggestive of offshore transport in the bottom Ekman layer.

The model calculation with no atmospheric forcing or sea ice produces a nearly identical transport across the 100 m isobath, so wind does not appear to be an important factor in offshore transport. Ekman pumping along the Chukchi slope west of Barrow Canyon is estimated to be of order $W_E = 20\text{m/yr}$, which produces a total of only 0.05 Sv of downward transport [*Meneghello et al.*, 2018], an order of magnitude smaller than the transport in Barrow Canyon. This Ekman pumping would also produce an offshore transport analogous to the southward Sverdrup transport in subtropical gyres. The magnitude of this transport can be estimated by a simple linear vorticity balance with $\beta_T V_T = f W_E / H$, where V_T is the cross-isobath velocity, $\beta_T = f \alpha / H$ is the topographic beta, α is the bottom slope, and H is the bottom depth. This simplifies to $V_T = W_E / \alpha$, which gives rise to a transport estimate of $\Psi = W_E L H / \alpha$, where L is the along-shelf length scale over which the Ekman pumping acts. The region of persistent downward Ekman pumping identified by *Meneghello et al.* [2018] lies along the outer shelf roughly between 160 W to 170W and 70 N to 72 N. The average bottom slope in this region between the 100 m and 200 m isobaths is $\mathcal{O}(0.002)$. A uniform Ekman pumping of $W_E = 20 \text{ m yr}^{-1}$ results in an offshore velocity of $\mathcal{O}(3.5 \times 10^{-4} \text{ m s}^{-1})$ and, taking an along-shelf distance of $L = 400$ km and an average bottom depth of $H = 150$ m, gives an offshore transport of $\mathcal{O}(0.02\text{Sv})$, more than an order of magnitude less than the cross topography transport in Barrow Canyon. Consideration of a nonzero vertical velocity at the bottom would reduce this transport even further. Even allowing for some shielding of the topographic slope effect due to stratification in summer, it is unlikely that this can account for significant cross topography transport.

Seasonality

It is well known that there is a strong seasonal cycle in the water mass properties in the Chukchi Sea and in the transport through Bering Strait [*Woodgate et al.*, 2005b,a]. The depth-integrated transport across the 100 m isobath as a function of month (averaged between the two years to reduce internal variability) and along-shelf distance shows that, while the magnitude of the transport across the topography changes with season,

422 the location does not (Fig. 9). Analysis as a function of depth also shows little season-
423 ality.

424 The transport across the 100 m isobath as a function of month and salinity is shown
425 in Fig. 10. The salinity generally falls between 32 and 34, although there are weaker fluxes
426 with lower salinity in summer and fall. The winter and early spring flux spans a wide
427 range of salinities while the late summer and fall salinity is more concentrated around
428 32.8. There is a negative salinity flux around 32 during January and February. This is
429 a signature of an eddy-driven exchange, with higher salinity water moving offshore and
430 lower salinity water moving onshore. There is no corresponding onshore net transport
431 across this isobath (Fig. 9).

432 The mean transport streamfunction shows that the off-shelf flow from Barrow Canyon
433 splits just seaward of the canyon – part of it turning towards the west and part towards
434 the east. A timeseries of the model transport at Barrow Canyon, through Bering Strait,
435 and westward across $x = 800$ km between the coast and $y = 1200$ km (which is in-
436 dicative of the Chukchi Slope Current) is shown in Fig. 11a. This is an annual cycle taken
437 as the average of the two years in the model integration. Each year is similar but we present
438 an average to reduce some of the internal variability. The bold dashed line is for the case
439 that has no seasonal cycle in restoring velocity at Bering Strait and no seasonal cycle
440 in wind-forcing, but includes the seasonal cycle in the inflowing temperature and salin-
441 ity at Bering Strait and in the atmospheric temperature and downward longwave and
442 shortwave radiation.

443 The model transport through Bering Strait is a minimum in winter at about 0.6
444 Sv and a maximum in summer at about 1.1 Sv. The transport through Barrow Canyon
445 (dash-dot line) shows a very similar seasonal cycle. It peaks roughly 2 weeks after Bering
446 Strait with almost 0.2 Sv less transport. This is the amount lost from the shelf to the
447 west of Barrow Canyon (Fig. 8). The westward transport in the Chukchi Slope Current
448 shows a peak in late summer and fall, about 2-3 months later than the peak transport
449 in Barrow Canyon. It is also more steady in winter and spring while the Bering Strait
450 and Barrow Canyon transports vary more sinusoidally year round.

451 Why is there a difference in the timing of the peak transport of the slope current
452 versus the Barrow Canyon outflow? One possibility is the influence of stratification. The
453 thin dashed line in Fig. 11a shows the change in density in the model from top to bot-
454 tom in Barrow Canyon. It is weakly stratified most of the year but has increased strat-
455 ification roughly between months 5 and 9. This corresponds well to the period of enhanced
456 westward transport of the slope current. During months 1 through 5 the transport through
457 Barrow Canyon is increasing while the westward transport offshore is fairly steady, so
458 the increase in westward transport in late summer is not simply a reflection of enhanced
459 transport in Barrow Canyon. The transport across the topography follows the seasonal
460 cycle (Fig. 9), so this change in westward transport is an indication of a change in the
461 direction of the offshore flow from stronger to the east in winter/spring to stronger to
462 the west in summer/fall. A heuristic explanation is that when the stratification is weak
463 the flow is influenced more by the topography. This suggests that the Pacific water on
464 the eastern flank of Barrow Canyon is more apt to follow the isobaths to the east into
465 the Beaufort Sea. By contrast, a more strongly stratified current is less trapped by the
466 bottom and more free to penetrate into the basin interior and turn towards the west. This
467 interpretation is supported by the calculation with no seasonal cycle in wind or the ve-
468 locity in Bering Strait to which the model is restored. The flow through Bering Strait
469 and Barrow Canyon has only a weak seasonal cycle (not shown), but the westward trans-
470 port in the Chukchi Slope Current displays nearly the same seasonal cycle as the stan-
471 dard calculation (bold dashed line).

472 With regard to the observed volume transports, we are constrained by the mea-
473 surement periods and spatial coverage of the moorings. The biggest limitation is that,

474 while there exist climatological records for Bering Strait, Barrow Canyon, and the Beau-
 475 fort shelfbreak jet, we have only a single year of data for the Chukchi Slope Current ar-
 476 ray, 2013-14. Furthermore, the central Barrow Canyon mooring failed during 2013-14,
 477 prohibiting a detailed comparison between the two sites for that year. Hence, the best
 478 we can do is consider a mix of climatology and the single year record for the Chukchi
 479 slope site. We note that since the model forcing is derived from the Bering Strait clima-
 480 tology as published in *Woodgate et al.* [2005b], this is what we present for the Bering Strait
 481 observations.

482 Despite these shortcomings, there are intriguing similarities between the measured
 483 and modeled Pacific water transports (Fig. 11b). In particular, Bering Strait and Bar-
 484 row Canyon peak in June and July, respectively, although the seasonal cycle in the ob-
 485 servations is stronger than that in the model (and the observed mean in Barrow Canyon
 486 is smaller than the model mean). Importantly, the peak in westward transport of the Chukchi
 487 Slope Current is 2-3 months later than this, consistent with the model. Furthermore, the
 488 slope current transport maximum occurs when the eastward transport of the Beaufort
 489 shelfbreak jet goes to zero in early fall. This supports the argument that a re-directioning
 490 of the flow out of Barrow Canyon is part of the reason for the seasonal timing of the slope
 491 current transport. Finally, we constructed a crude measure of the mid water column strat-
 492 ification in Barrow Canyon (centered at 60 m depth) using the mooring MicroCAT data,
 493 which reveals a peak in stratification in September/October, i.e. later than transport peak
 494 in Barrow Canyon but close to the Chukchi Slope Current peak (not shown). This of-
 495 fers support for the notion that the lack of bottom trapping allows more of the outflow
 496 from Barrow Canyon to veer westward at this time of year. While there are discrepan-
 497 cies between the model and data, the basic seasonality is encouragingly similar in both.

498 *Pacific Water tracer*

499 The exchange depicted in Fig. 8 represents the source of Pacific origin waters to
 500 the halocline. The ventilation on the shelf and the pathways into the interior are diag-
 501 nosed by consideration of two passive tracers in the model. The first marks Pacific ori-
 502 gin waters advected into the Chukchi Sea within the forcing region in Bering Strait. It
 503 is given a value of 1 within the strait but is otherwise unforced outside of the strait. The
 504 second passive tracer is continuously set to 1 at the surface within the Chukchi Sea (iso-
 505 bath shallower than 60 m) and set to zero below the surface layer within the forcing re-
 506 gion in Bering Strait. This may be thought of as a ventilation tracer since it marks wa-
 507 ters on the shelf that were within the mixed layer. Low values on the shelf indicate wa-
 508 ters that were advected through Bering Strait but remained unventilated by contact with
 509 the surface layer.

510 A snapshot of the Pacific water tracer at 47.5 m depth near the shelfbreak at the
 511 end of the model calculation is shown in Fig. 12. Areas shallower than 47.5 m are shaded
 512 gray. Over most of the region, the tracer remains shallower than the 100 m isobath. How-
 513 ever, at and to the east of Barrow Canyon large amounts of shelf water are advected off-
 514 shore. The primary injection site is along the eastern flank of Barrow Canyon, as indi-
 515 cated in Fig. 8, although some plumes and eddies are seen forming farther to the east.
 516 (Note that eddies can flux tracers from the shelf to the interior but have no net volume
 517 flux.) The tracer breaks up into mesoscale eddies and filaments once in the interior and
 518 is transported both east and west from Barrow Canyon, consistent with the transport
 519 streamfunction in Fig. 4. The weaker offshore flux near $x=600$ km is the small outflow
 520 from Hanna Canyon. Importantly, there is a plume of Pacific water offshore of the 300
 521 m isobath extending westward all the way to the Northwind Ridge, which is consistent
 522 with an eastern source and westward flow in the Chukchi Slope Current, rather than a
 523 local offshore flux west of $x=600$ km.

524 The average of the Pacific water tracer as a function of distance from the 75 m iso-
 525 bath is shown in Fig. 7d. There are two local maxima: one in the vicinity of the shelf-

526 break corresponding to the eastward-flowing shelfbreak jet, and the other centered near
 527 80 km in the Chukchi Slope Current. The tracer concentration is a maximum around
 528 100 m depth with lower concentrations near the surface. This directly connects the sub-
 529 surface waters of the Chukchi Slope Current with the Barrow Canyon outflow. The tracer
 530 is smaller in the upper layer due to the influence of fresh water from ice melt getting mixed
 531 downwards. This is consistent with the observations of *Corlett and Pickart* [2017]. The
 532 resulting density structure supports a positive vertical shear, giving a maximum veloc-
 533 ity near the surface, yet these waters did not predominantly come from Bering Strait in
 534 the two year period of integration, leading to the subsurface maximum in Pacific water
 535 tracer.

536 Evidence of where this offshore flux takes place is indicated by the total transport
 537 of Pacific water tracer across the 60, 100, 200, and 300 m isobaths (Fig. 13). The color
 538 of the bold lines represents the total transport of Pacific water tracer across each iso-
 539 bath, integrated from the surface to the bottom, starting from zero at the western bound-
 540 ary. The regions of cross topography flux are indicated by a change in color from dark to
 541 light. The 60 m isobath has a large southward excursion in Herald Canyon, and we
 542 find about 0.2 Sv of cross topography flow within the canyon, with some of this return-
 543 ing to shallower water just east of the Canyon. From here, there is a more subtle increase
 544 towards the east, then an abrupt increase to 0.65 Sv within Barrow Canyon. Slightly deeper,
 545 at the 100 m isobath, there is only weak cross isobath transport west of $x=600$ km, in-
 546 dicating that most of the transport across the 60 m isobath in Herald Canyon turns to-
 547 wards the east and remains onshore of the 100 m isobath. There is then a gradual in-
 548 crease to the east before another abrupt increase to 0.65 Sv within Barrow Canyon. The
 549 two deeper isobaths, 200 and 300 m, show very little cross isobath transport west of Bar-
 550 row Canyon.

551 This total cross topography transport can be decomposed into mean and eddy con-
 552 tributions. We find that it is dominated by the mean flow, although the eddy transports
 553 are as large as 0.1 Sv within Barrow Canyon (Fig. 14). There are also weaker offshore
 554 eddy fluxes between $x=500$ km and Barrow Canyon, as suggested by Fig. 12.

555 *Extent of ventilation on the shelf*

556 The Pacific water tracer indicates where these waters enter the basin interior, but
 557 not where, or even if, these waters were ventilated within the Chukchi Sea. The prod-
 558 uct of the Pacific water tracer and the ventilation tracer is an indication of waters that
 559 flowed through Bering Strait and were ventilated, or were within the surface mixed layer,
 560 within the Chukchi Sea. Unventilated Pacific water is the product of the Pacific water
 561 tracer and one minus the ventilation tracer. The volume of this unventilated water is shown
 562 in Fig. 15 as a function of time. The blue line is calculated over the region between the
 563 Bering Strait inflow and $y = 600$ km (i.e. south of Pt. Hope, see Fig. 1). Initially there
 564 is none of this water because in winter the water column is well mixed throughout the
 565 southern Chukchi Sea. However, in late spring the flow through Bering Strait becomes
 566 stratified and unventilated water starts to be advected into the southern Chukchi Sea.
 567 This peaks in late summer, is rapidly reduced in fall, and eliminated by the end of the
 568 year. This is a result of ice formation and brine rejection, which drives convective mix-
 569 ing to the bottom.

570 The green line is the same calculation for the region south of $y = 800$ km (roughly
 571 the latitude of Icy Cape, Fig. 1). We find a similar temporal evolution but larger vol-
 572 ume. This indicates that the unventilated water is advected beyond $y = 600$ km be-
 573 fore winter sets in. The volume of unventilated water over the entire Chukchi shelf (red
 574 line), defined as everywhere shallower than 100 m, is larger still than that found south
 575 of $y = 800$ km. Importantly, some volume of this water remains between $y = 800$ km
 576 and the 100 m isobath all year round. In late fall the volume south of 800 km is reduced
 577 more rapidly than the volume shallower than 100 m. This indicates that the unventi-

578 lated water is advected onto the outer Chukchi shelf, where it is at least partly shielded
 579 from convection. The volume of unventilated water at depth greater than 100 m steadily
 580 increases from the time the unventilated water first reaches the shelfbreak at 1/2 year
 581 until the end of the calculation (black line). The rate of increase corresponds to a mean
 582 cross topography flux of about 0.17 Sv and is nearly steady in time (i.e. no seasonal cy-
 583 cle). Recall that the mean Pacific Water transport across the 100 m isobath is about 0.65
 584 Sv, meaning that approximately 25% of the transport of Pacific water into the Canada
 585 Basin is not ventilated in the Chukchi Sea. The advective speeds through the Chukchi
 586 Sea are sufficiently fast that water parcels can transit the shelf before winter convection
 587 sets in. This differs from the subtropical gyres of the major ocean basins where the ad-
 588 vective speeds are slow enough that only parcels that leave the mixed layer within a one
 589 or two month period at the end of winter are able to avoid getting entrained into the mixed
 590 layer in the following winter, thus resulting in a bias of the permanent thermocline prop-
 591 erties towards those found at the end of winter in the mixed layer [Stommel, 1979; Williams
 592 *et al.*, 1995].

593 *Relation to the Beaufort Gyre*

594 It is logical to consider the relationship between the Chukchi Slope Current and
 595 the Beaufort Gyre. The flow is westward and surface intensified for both features, how-
 596 ever there are important differences. To the extent that the circulation dynamics in the
 597 basin interior are linear, we may consider the fully forced problem as the sum of the wind-
 598 and buoyancy-forced interior circulation and the circulation that results from the flow
 599 through Bering Strait in the absence of any atmospheric forcing. A model run identi-
 600 cal to the fully-forced case but with a closed Bering Strait produces an anticyclonic Beau-
 601 fort Gyre (Fig. 16a) much as is found in the fully forced case. The primary difference
 602 in the basin interior is that, in the absence of Bering Strait inflow, there is westward flow
 603 offshore of the Beaufort slope, to the east of Barrow Canyon ($900km < x < 1300km$),
 604 whereas the fully forced circulation shows weak eastward flow. The case with only flow
 605 through Bering Strait (Fig. 16b) produces the three main branches flowing through the
 606 Chukchi Sea and a strong transport through Barrow Canyon (the flow through the Chukchi
 607 Sea is shifted to the east in the fully forced case as a result of the cyclonic wind stress
 608 curl [Spall, 2007]). The flow exits Barrow Canyon and most of it crosses the isobaths,
 609 penetrates into the southern part of the basin, and turns to the east before exiting the
 610 domain.

611 If the flow were purely linear, the sum of these two solutions would be equal to the
 612 solution for the fully forced case. While the model is not linear, we can see that the ten-
 613 dency of adding these solutions together is to produce a large-scale circulation that re-
 614 sembles the fully forced case. Off the Beaufort shelf the eastward transport of the Bering
 615 Strait case will diminish the westward transport of the wind-driven gyre, particularly
 616 nearer the coast, resulting in only weak westward or even eastward flow. This is largely
 617 what we find for the fully forced calculation. This is also true of the observations: there
 618 is weak eastward flow offshore of the Beaufort shelfbreak jet at least out to the 700 m
 619 isobath (Fig. 6b; see also *Nikolopoulos et al.* [2009]). To the west of Barrow Canyon, the
 620 Bering Strait forced case produces no flow, so the linear sum would have the same west-
 621 ward transport as the Beaufort Gyre case, which is also consistent with the fully-forced
 622 model result. However, the source of this westward flow is Barrow Canyon, not a recir-
 623 culation of the Beaufort Gyre water from the east.

624 The linear sum is useful for understanding the pressure field but it does not directly
 625 apply to the tracer field. The Chukchi Slope Current is a well defined feature in the full
 626 model with an offshore edge that is distinguishable from the southern portion of the Beau-
 627 fort Gyre (Fig. 7). This most likely relates to the distinct core of Pacific water (Fig. 7c,
 628 Figs. 4 and 5 of *Corlett and Pickart* [2017]), which will alter the velocity profile through
 629 the thermal wind balance. Also, as seen above, the seasonal variability of the westward

630 transport appears to originate from the Chukchi Sea in the model as well as the obser-
631 vations; i.e., it is not an inherent part of the wind-driven Beaufort Gyre.

632 5 Summary and Discussion

633 The primary objective of this study was to understand where and how Pacific Wa-
634 ters enter the interior of the Canada Basin. This process is essential for maintenance of
635 the halocline, providing nutrients and zooplankton to the local ecosystem, and insula-
636 tion of sea ice from the warm Atlantic Waters below. It has long been known that Pa-
637 cific Waters get modified on the Chukchi shelf and enter the basin interior, but the means
638 by which this occurs is not well understood.

639 The primary pathway in a high resolution regional ocean/ice model was shown to
640 be nonlinear advection through Barrow Canyon. The transports in the model Chukchi
641 Sea, and at three key locations – Barrow Canyon, the Beaufort shelfbreak, the Chukchi
642 shelfbreak and slope – are consistent with observational estimates, providing confidence
643 in the utility of the model fields. After crossing the topography in Barrow Canyon, most
644 of the transport turns to the west and forms the Chukchi Slope Current. Similar cross-
645 shelf flow and westward transport have been previously found in numerical models [*Zhang*
646 *et al.*, 2016; *Aksenov et al.*, 2016; *Watanabe et al.*, 2017], but their focus was not on this
647 process and its role in providing source waters to the halocline. We consider this trans-
648 port to have replaced Beaufort Gyre water that would have been advected from the east
649 in the absence of the flow out of Barrow Canyon. Our finding, in both observations and
650 the model, that the flow east of Barrow Canyon and offshore of the shelfbreak is weakly
651 towards the east supports this interpretation. Dynamically, one can think of this circu-
652 lation as the linear sum of the wind-driven anticyclonic gyre and the cross-topography
653 flow exiting Barrow Canyon that ultimately is driven by flow through Bering Strait. While
654 the westward flow is balanced by the the sea surface height slope and the anticyclonic
655 wind stress curl, as is the Beaufort Gyre, the source region and water mass properties
656 are different from the large-scale Beaufort Gyre circulation and so we consider this a dis-
657 tinct current.

658 This advective process is operative at all times of year, although the peak westward
659 transport in the Chukchi Slope Current occurs in late summer, several months later than
660 the peak transport through Bering Strait. The delay appears to be related to stronger
661 stratification, weaker topographic control, and more offshore transport at the end of sum-
662 mer. Although we lack a simple theoretical model, the basic mechanism here is nonlin-
663 ear advection as a result of topographic steering on the shelf guiding the flow into the
664 narrow Barrow Canyon. Based on the model calculations and a linear vorticity scaling,
665 wind-forcing plays no role in this process. We find no evidence for wind-driven exchange
666 broadly distributed along the shelfbreak, analogous to the mid-latitude subtropical gyre
667 subduction process, as proposed by *Timmermans et al.* [2014, 2017]. This is likely due
668 to a combination of the very strong topographic beta, which minimizes the ocean response
669 to Ekman pumping, and the moderation of stress transmitted to the ocean current be-
670 cause of the seasonally concentrated sea ice cover [*Meneghello et al.*, 2018].

671 Acknowledgments

672 This study was supported by the National Science Foundation under grants PLR-1415489
673 and OCE-1533170 (MAS), the Bureau of Ocean and Energy Management under contract
674 M12AC00008 (RSP and ML), the National Oceanic and Atmospheric Administration
675 grant NA16OAR4310248 (PL). The authors would like to thank two anonymous review-
676 ers for their helpful comments and suggestions for improving this manuscript.

677 Data from the Beaufort slope array is available at <http://aon.whoi.edu>. The Chukchi
678 slope mooring data is available through the Bureau of Ocean and Energy Management

679 (https://www.boem.gov). The Chukchi slope hydrographic and shipboard ADCP data
 680 are available through <http://hdl.handle.net/1912/8170>. The Barrow Canyon mooring
 681 data can be found at http://www.jamstec.go.jp/arctic/data_archive_work/mooring/mooring_index.html.
 682 The Bering Strait mooring data are available at [http://psc.apl.washington.edu/HLD/Bstrait/
 683 Data/BeringStraitMooringDataArchive.html](http://psc.apl.washington.edu/HLD/Bstrait/Data/BeringStraitMooringDataArchive.html). The numerical model input parameters,
 684 forcing fields, and configuration are available at the NSF Arctic Data Center,
 685 <https://arcticdata.io/catalog/#view/doi:10.18739/A21C4S>.

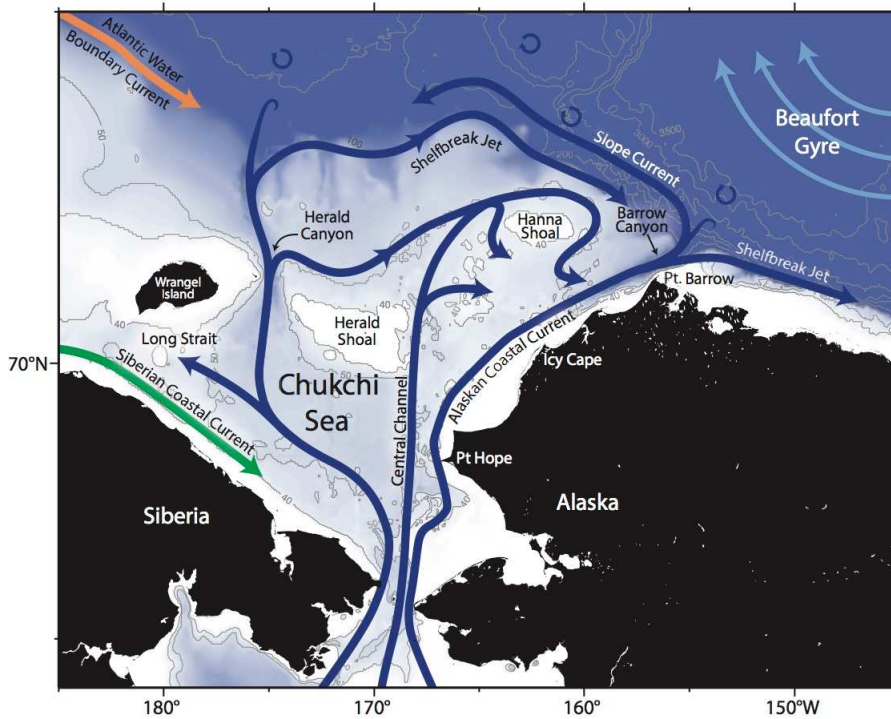
686 References

- 687 Aksenov, Y., M. Karcher, A. Proshutinsky, R. Gerdes, B. de Cuevas, E. Golubeva,
 688 F. Kauker, A. T. Nguyen, G. A. Platov, M. Wadley, E. Watanabe, A. C. Cow-
 689 ard, and A. J. G. Nurser (2016), Arctic pathways of Pacific Water: Arctic
 690 Ocean Model Intercomparison experiments, *J. Geophys. Res.*, *121*, 27–59, doi:
 691 doi:10.1002/2015JC011299.
- 692 Ashjian, C. J., S. R. Braund, R. G. Campbell, J. C. George, J. Kruse,
 693 W. Maslowski, S. E. Moore, C. R. Nicolson, S. R. Okkonen, B. F. Sherr, E. B.
 694 Sherr, and Y. H. Spitz (2010), Climate variability, oceanography, bowhead whale
 695 distribution, and Iñupiat subsistence whaling near Barrow, Alaska, *Arctic*, *63*(2),
 696 179–194.
- 697 Brugler, E., R. Pickart, G. Moore, S. Roberts, T. Weingartner, and H. Statscewich
 698 (2014), Seasonal to Interannual Variability of the Pacific Water Boundary Current
 699 in the Beaufort Sea, *Prog. Oceanogr.*, *127*, 1–20.
- 700 Codispoti, L. A., C. Flagg, V. Kelly, and J. H. Swift (2005), Hydrographic condi-
 701 tions during the 2002 SBI process experiments, *Deep-Sea Res. II*, *52*, 3199–3226.
- 702 Corlett, W., and R. S. Pickart (2017), The Chukchi Slope Current, *Progress in*
 703 *Oceanography*, *153*, 50–65.
- 704 Cross, J., J. Mathis, R. S. Pickart, and N. Bates (2017), Formation and transport of
 705 corrosive water in the Pacific Arctic region, *Deep-Sea Res. II*, p. in press.
- 706 Gong, D., and R. S. Pickart (2015), Summertime circulation in the eastern Chukchi
 707 Sea, *Deep-Sea Research Part II: Topical Studies in Oceanography*, *118*, 18–31,
 708 doi:10.1016/j.dsr2.2015.02.006.
- 709 Hopcroft, R. R., K. N. Kosobokova, and A. I. Pinchuk (2010), Zooplankton commu-
 710 nity patterns in the Chukchi Sea during summer 2004, *Deep Sea Research Part II:
 711 Topical Studies in Oceanography*, *57*(1-2), 27–39, doi:10.1016/j.dsr2.2009.08.003.
- 712 Hunke, E. C., and J. K. Dukowicz (1997), An elastic-viscous-plastic modle for sea ice
 713 dynamics, *J. Phys. Oceanogr.*, *27*, 1849–1867.
- 714 Itoh, M., S. Nishino, Y. Kawaguchi, and T. Kikuchi (2013), Barrow Canyon volume,
 715 heat, and freshwater fluxes revealed by long-term mooring observations between
 716 2000 and 2008, *Journal of Geophysical Research: Oceans*, *118*(9), 4363–4379,
 717 doi:10.1002/jgrc.20290.
- 718 Jackett, D. R., and T. J. McDougall (1995), Minimal adjustment of hydrographic
 719 profiles to achieve static stability, *J. Atmos. Ocean. Tech.*, *12*, 381–389.
- 720 Large, W. G., and S. Pond (1981), Open ocean momentum flux measurements in
 721 moderate to strong winds, *J. Phys. Oceanogr.*, *11*, 324–336.
- 722 Large, W. G., J. C. McWilliams, and S. C. Doney (1994), Oceanic vertical mixing:
 723 A review and a model with a nonlocal boundary layer parameterization, *Rev.
 724 Geophys.*, *32*, 363–403.
- 725 Li, M., and R. Pickart (2017), Circulation of the Chukchi Sea shelfbreak and slope
 726 from moored timeseries, *Alaska Marine Science Symposium, collected abstracts*.
- 727 Li, M., R. Pickart, M. A. Spall, T. Weingartner, P. Lin, G. W. K. Moore, and Y. Qi
 728 (submitted), Circulation of the Chukchi Sea shelfbreak and slope from moored
 729 timeseries, *Prog. Oceanogr.*

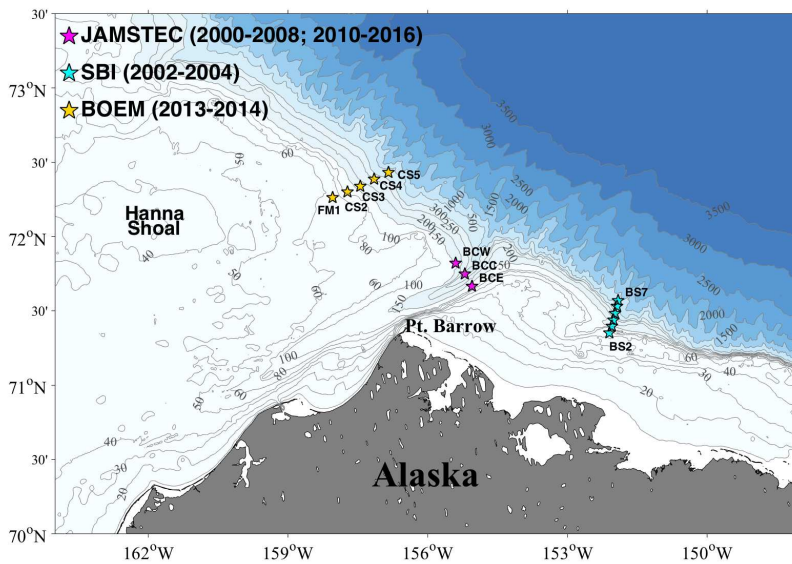
- 730 Manley, T. O., and K. Hunkins (1985), Mesoscale eddies of the Arctic Ocean, *J.*
731 *Geophys. Res.*, *90*, 4911–4930.
- 732 Marshall, J., C. Hill, L. Perelman, and A. Adcroft (1997), Hydrostatic, quasi-
733 hydrostatic, and non-hydrostatic ocean modeling, *J. Geophys. Res.*, *102*, 5733–
734 5752.
- 735 Mathis, J. T., R. S. Pickart, D. A. Hansell, D. Kadko, and N. R. Bates (2007), Eddy
736 transport of organic carbon and nutrients from the Chukchi shelf into the deep
737 Arctic basin, *J. Geophys. Res.*, *112*, doi:10.1029/2006JC003899.
- 738 Meneghello, G., J. Marshall, M.-L. Timmermans, and J. Scott (2018), Observations
739 of Seasonal Upwelling and Downwelling in the Beaufort Sea Mediated by Sea Ice,
740 *J. Phys. Oceanogr.*, *48*, 795–805.
- 741 Mizobata, K., E. Watanabe, and N. Kimura (2016), Wintertime variability of
742 the Beaufort gyre in the Arctic Ocean derived from CryoSat-2/SIRAL ob-
743 servations, *Journal of Geophysical Research C: Oceans*, *121*, 1685–1699, doi:
744 10.1002/2015JC011218.
- 745 Moore, G. W. K. (2012), Decadal variability and a recent amplification of the
746 summer {B}eaufort {S}ea {H}igh, *Geophysical Research Letters*, *39*, doi:
747 doi:10.1029/2012GL051570.
- 748 Nelson, R. J., E. C. Carmack, F. A. McLaughlin, and G. A. Cooper (2009), Pene-
749 tration of pacific zooplankton into the western arctic ocean tracked with molec-
750 ular population genetics, *Marine Ecology Progress Series*, *381*, 129–138, doi:
751 10.3354/meps07940.
- 752 Nikolopoulos, A., R. Pickart, P. Fratantoni, K. Shimada, D. Torres, and E. Jones
753 (2009), The western Arctic boundary current at 152°W: Structure, variability, and
754 transport, *Deep-Sea Research II*, *56*, 1164–1181.
- 755 Panteleev, G., D. A. Nechaev, A. Proshutinsky, R. Woodgate, and J. Zhang (2010),
756 Reconstruction and analysis of the Chukchi Sea circulation in 1990–1991, *Journal*
757 *of Geophysical Research: Oceans*, *115*(8), 1–22, doi:10.1029/2009JC005453.
- 758 Paquette, R., and R. H. Bourke (1974), Observations on the coastal current of
759 arctic alaska, *Journal of Marine Research*, *32*(2), 195–207.
- 760 Pickart, R., and G. Stossmeister (2009), Outflow of water from the Chukchi Sea to
761 the Arctic Ocean, *Chinese Journal of Polar Science*, *9*, 135–148.
- 762 Pickart, R., L. Pratt, D. Torres, T. Whitledge, A. Proshutinsky, K. Aagaard, T. Ag-
763 new, G. Moore, and H. Dail (2010), Evolution and dynamics of the flow through
764 Herald Canyon in the Western Chukchi Sea, *Deep-Sea Research II*, *57*, 5–26.
- 765 Pickart, R. S., T. J. Weingartner, S. Zimmermann, D. J. Torres, and L. J. Pratt
766 (2005), Flow of winter-transformed Pacific water into the western Arctic, *Deep Sea*
767 *Res. II*, *52*, 3175–3198.
- 768 Pickart, R. S., M. A. Spall, G. Moore, T. J. Weingartner, R. A. Woodgate, K. Aa-
769 gaard, and K. Shimada (2011), Upwelling in the alaskan beaufort sea: Atmo-
770 spheric forcing and local versus non-local response, *Progress in Oceanography*, *88*,
771 78–100.
- 772 Pickart, R. S., G. W. K. Moore, C. Mao, F. Bahr, C. Nobre, and T. J. Weingartner
773 (2016), Circulation of winter water on the Chukchi shelf in early Summer,
774 *Deep-Sea Research Part II: Topical Studies in Oceanography*, *130*, 56–75, doi:
775 10.1016/j.jdsr.2.2016.05.001.
- 776 Proshutinsky, A., R. H. Bourke, and F. A. McLaughlin (2002), The role of the Beau-
777 fort Gyre in Arctic climate variability: Seasonal to decadal climate scales, *Geo-*
778 *phys. Res. Lett.*, *29*(23), 15–1–15–4, doi:10.1029/2002GL015847.
- 779 Proshutinsky, A., R. Krishfield, M. L. Timmermans, J. Toole, E. Carmack,
780 F. McLaughlin, W. J. Williams, S. Zimmermann, M. Itoh, and K. Shi-
781 mada (2009), Beaufort {G}yre freshwater reservoir: {S}tate and vari-
782 ability from observations, *Journal of Geophysical Research*, *114*, C00A10,
783 doi:10.1029/2008JC005104.

- 884 Proshutinsky, A., D. Dukhovskoy, M.-l. Timmermans, R. Krishfield, J. L. Bamber,
885 and A. Proshutinsky (2015), Arctic circulation regimes, *Phil. Trans. R. Soc. A*,
886 *373*.
- 887 Semtner, A. J. (1976), A model for the thermodynamic growth of sea ice in numeri-
888 cal investigations of climate, *J. Phys. Oceanogr.*, *6*, 379–389.
- 889 Smagorinsky, J. (1963), General circulation experiments with the primitive equa-
890 tions:I. The basic experiment, *Mon. Wea. Rev.*, *91*, 99–164.
- 891 Spall, M. A. (2007), Circulation and water mass transformation in a model of the
892 chukchi sea, *J. Geophys. Res.*, *112*, doi:10.1029/2005JC002,264.
- 893 Spall, M. A., R. S. Pickart, P. S. Fratantoni, and A. J. Plueddemann (2008), West-
894 ern Arctic Shelfbreak Eddies: Formation and Transport, *J. Phys. Oceanogr.*, *38*,
895 1644–1668.
- 896 Stabeno, P., N. Kachel, C. Ladd, and R. Woodgate (2018), Flow patterns in the
897 eastern Chukchi Sea: 2010-2015, *J. Geophys. Res.*, *123*, 1177–1195.
- 898 Steele, M., R. Morley, and W. Ermold (2001), PHC: A global ocean hydrography
899 with a high quality Arctic Ocean, *Journal of Climate*, *14*, 2079–2087.
- 900 Stommel, H. (1979), Determination of watermass properties of water pumped down
901 from the Ekman layer to the geostrophic flow below, *Proc. Natl. Acad. Sci. U. S.*,
902 *76*, 3051–3055.
- 903 Timmermans, M.-L., A. Proshutinsky, E. Golubeva, J. M. Jackson, R. Krishfield,
904 M. McCall, G. Platov, J. Toole, W. Williams, T. Kikuchi, and S. Nishino (2014),
905 Mechanisms of Pacific Summer Water variability in the Arctic’s Central Canada
906 Basin, *J. Geophys. Res.*, *119*, 7523–7548.
- 907 Timmermans, M.-L., J. Marshall, A. Proshutinsky, and J. Scott (2017), Season-
908 ally derived components of the Canada Basin halocline, *Geophys. Res. Lett.*, *44*,
909 5008–5015.
- 910 Wassmann, P., K. N. Kosobokova, D. Slagstad, K. F. Drinkwater, R. R. Hopcroft,
911 S. E. Moore, I. Ellingsen, R. J. Nelson, E. Carmack, E. Popova, and J. Berge
912 (2015), The contiguous domains of Arctic Ocean advection: Trails of life and
913 death, *Progress in Oceanography*, *139*, 42–65, doi:10.1016/j.pocean.2015.06.011.
- 914 Watanabe, E., J. Onodero, M. Itoh, S. Nishino, and T. Kikuchi (2017), Winter
915 transport of subsurface warm water toward the Arctic Chukchi Borderland, *Deep*
916 *Sea Res. I*, p. doi:10.1016/j.dsr.2017.08.009.
- 917 Weingartner, T. J., K. Aagaard, R. Woodgate, S. Danielson, Y. Sasaki, , and
918 D. Cavalieri (2005), Circulation on the north central Chukchi shelf, *Deep Sea*
919 *Res. II*, *52*, 3150–3174.
- 920 Weingartner, T. J., C. Irvine, E. Dobbins, S. Danielson, L. DeSousa, B. Adams,
921 R. Suydam, and W. Neatok (2015), Satellite-tracked Drifter Measurements in the
922 Chukchi and Beaufort Seas., *Technical Report 2015-022. Bureau of Ocean Energy*
923 *Management*.
- 924 Weingartner, T. J., R. Potter, C. A. Stoudt, E. L. Dobbins, H. Statscewich, P. R.
925 Winsor, T. D. Mudge, and K. Borg (2017), Transport and thermohaline variabil-
926 ity in Barrow Canyon on the Northeastern Chukchi shelf, *Journal of Geophysical*
927 *Research C: Oceans*, *122*, 2017–2033, doi:10.1002/2016JC012636.
- 928 Williams, R. G., M. A. Spall, and J. C. Marshall (1995), Does Stommel’s mixed-
929 layer ‘demon’ work?, *J. Phys. Oceanogr.*, *25*, 3089–3102.
- 930 Winsor, P., and D. C. Chapman (2004), Pathways of Pacific water across
931 the Chukchi Sea: A numerical model study, *J. Geophys. Res.*, *109*, doi:
932 doi:10.1029/2003JC001962.
- 933 Winton, M. (2000), A reformulated three-layer sea ice model, *J. Atmos. Oceanic*
934 *Tech.*, *17*, 525–531.
- 935 Woodgate, R. A. (2017), Increases in the Pacific inflow to the Arctic from 1990
936 to 2015, and insights into seasonal trends and driving mechanisms from
937 year-round Bering Strait mooring data, *Prog. Oceanogr.*, *160*, 124–154, doi:

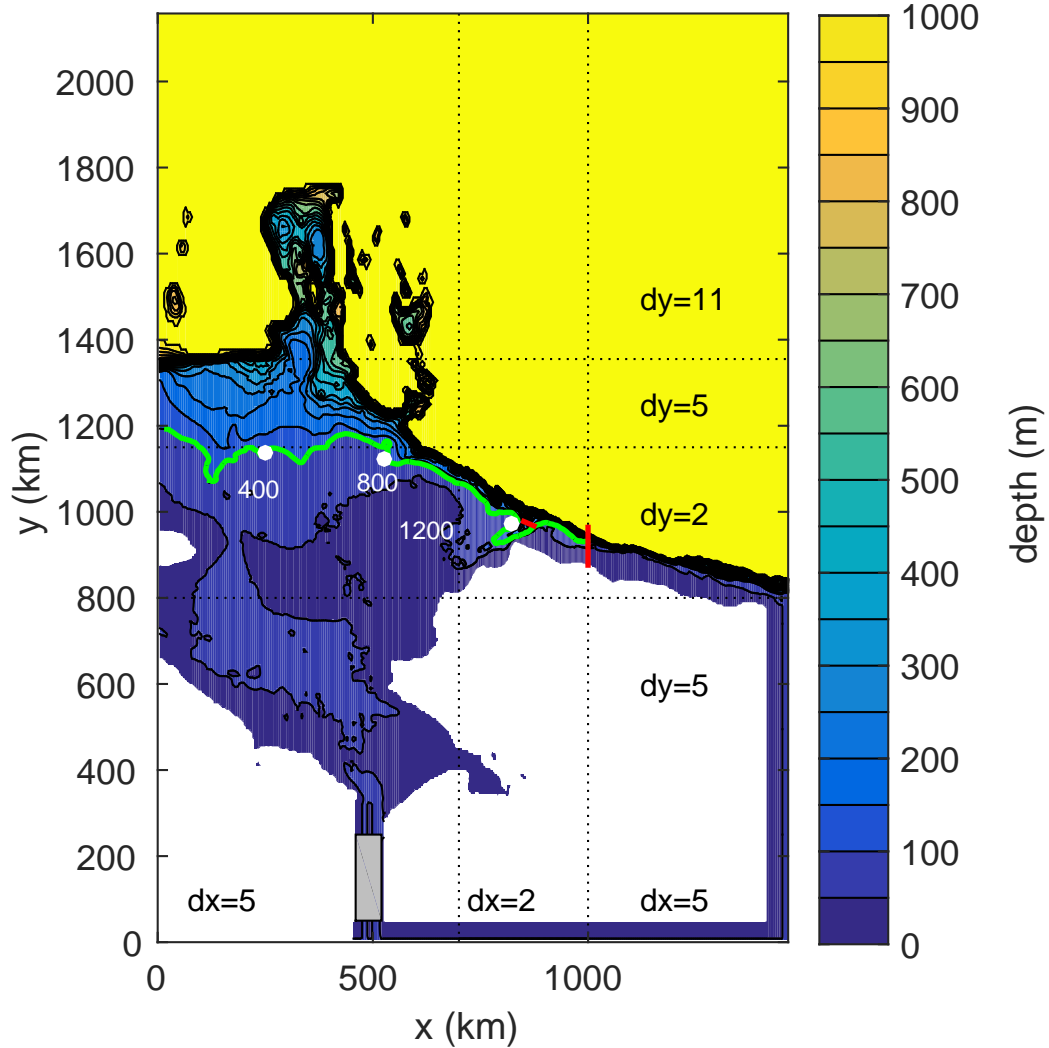
- 838 10.1016/j.pocean.2017.12.007.
- 839 Woodgate, R. A., K. Aagaard, and T. Weingartner (2005a), A year in the physical
840 oceanography of the Chukchi Sea, *Deep Sea Res. Part II*, *52*, 3116–3149.
- 841 Woodgate, R. A., K. Aagaard, and T. Weingartner (2005b), Monthly temperature,
842 salinity, and transport variability in the bering strait through flow, *Geophys. Res.*
843 *Lett.*, *32*, doi:10.1029/2004GL021,880.
- 844 Woodgate, R. A., T. J. Weingartner, and R. Lindsay (2012), Observed increases
845 in Bering Strait oceanic fluxes from the Pacific to the Arctic from 2001 to 2011
846 and their impacts on the Arctic Ocean water column, *Geophys. Res. Lett.*, *39*,
847 doi:doi:10.1029/2012GL054092.
- 848 Zhang, J., M. Steele, K. Runciman, S. Dewey, J. Morison, C. Lee, L. Rainville,
849 S. Cole, R. Krishfield, M.-L. Timmermans, and J. Toole (2016), The Beaufort
850 Gyre intensification and stabilization: A model-observation synthesis, *J. Geophys.*
851 *Res.*, *121*, 7933–7952.
- 852 Zhao, M., M.-L. Timmermans, S. Cole, R. Krishfield, A. Proshutinsky, and J. Toole
853 (2014), Characterizing the eddy field in the Arctic Ocean, *J. Geophys. Res.*, *119*,
854 8800–8817.



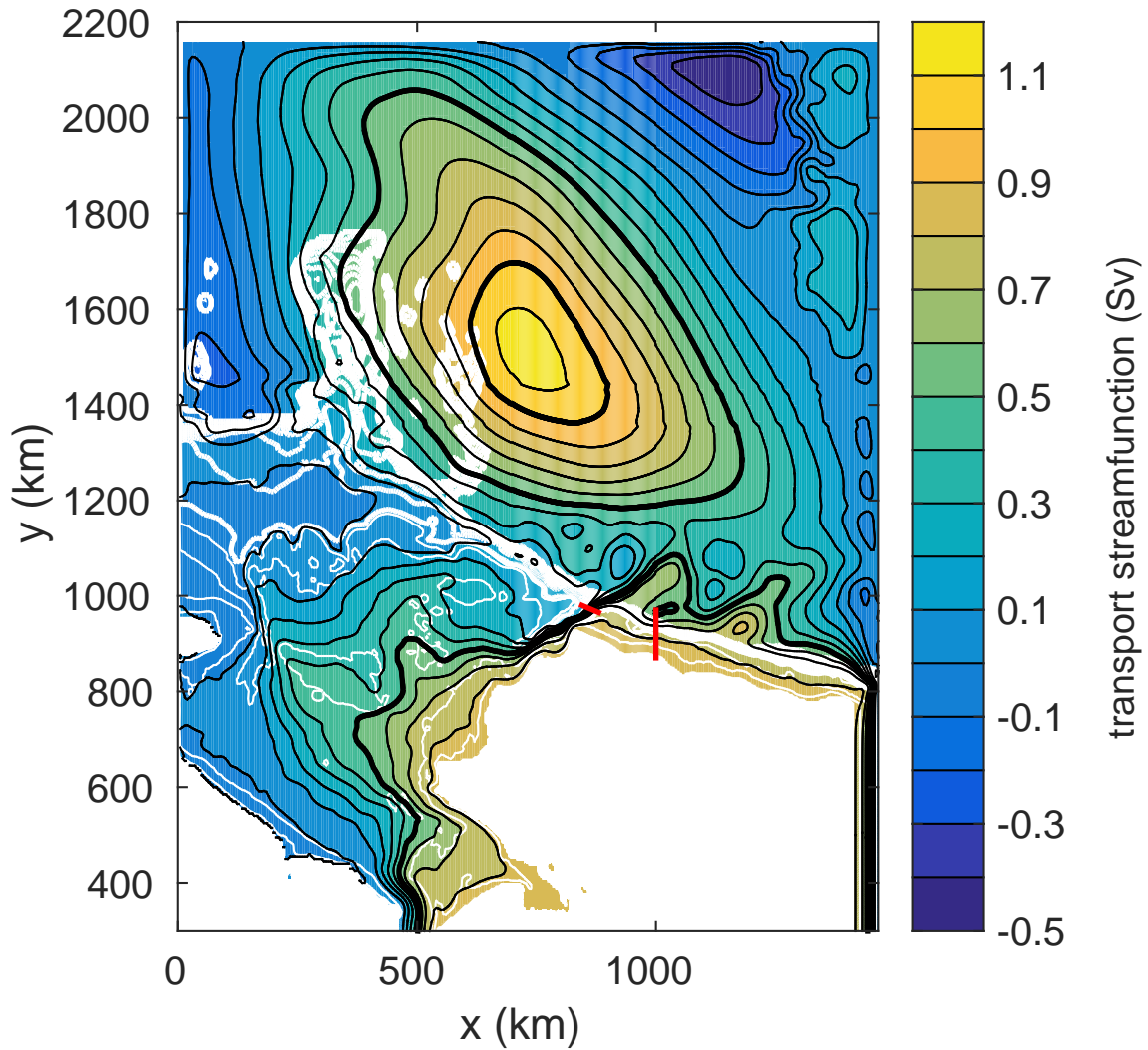
855 **Figure 1.** Schematic circulation of the Chukchi Sea and place names, after *Corlett and*
 856 *Pickart [2017]*



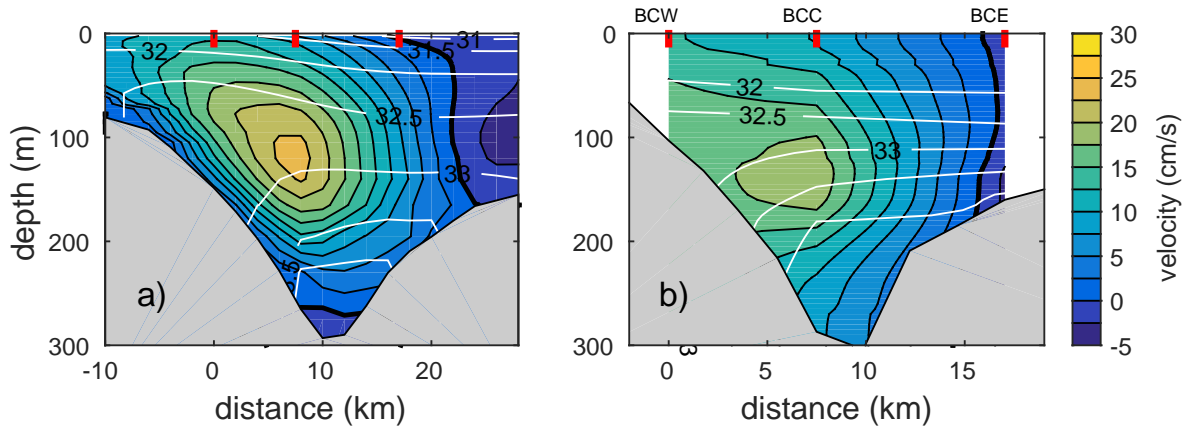
857 **Figure 2.** Locations of the three mooring arrays whose data are used in the study. See the
 858 legend for the time periods of the measurements. JAMSTEC = Japan Agency for Marine-Earth
 859 Science and Technology; SBI = Western Arctic Shelf-Basin Interactions Program; BOEM =
 860 Bureau of Ocean Energy and Management.



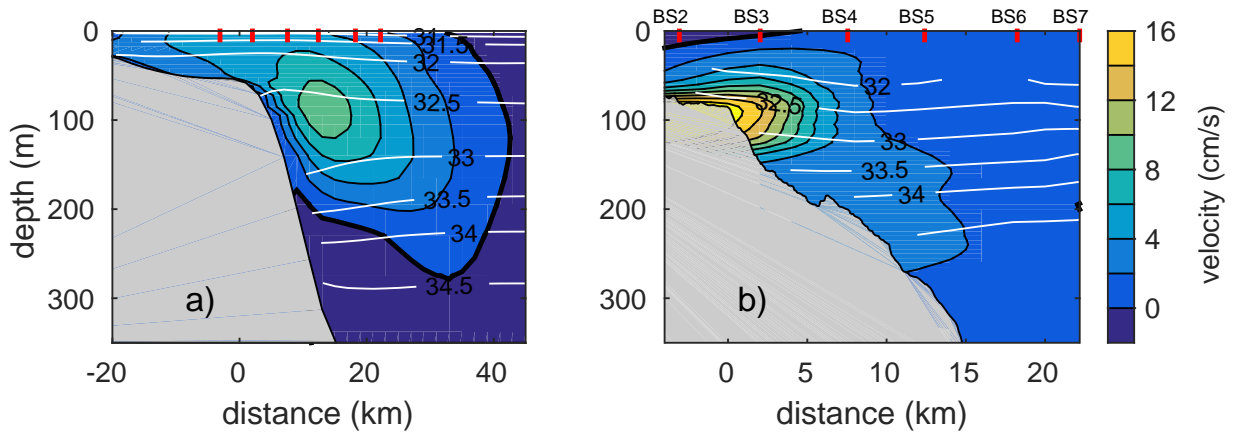
861 **Figure 3.** The model domain and bottom topography. The grid spacing is variable, as indicated on the figure with transitions marked by the dotted lines. The gray box near $x = 500$ km,
 862 $y = 200$ km is the region of restoring terms forcing the flow through Bering Strait. The two red
 863 lines mark the locations of the sections shown in Figs. 5 and 6. The bold green line indicates
 864 the 100 m isobath, and the white dots indicate distance along that isobath from the western
 865 boundary of the model, plotted in Fig. 8.
 866



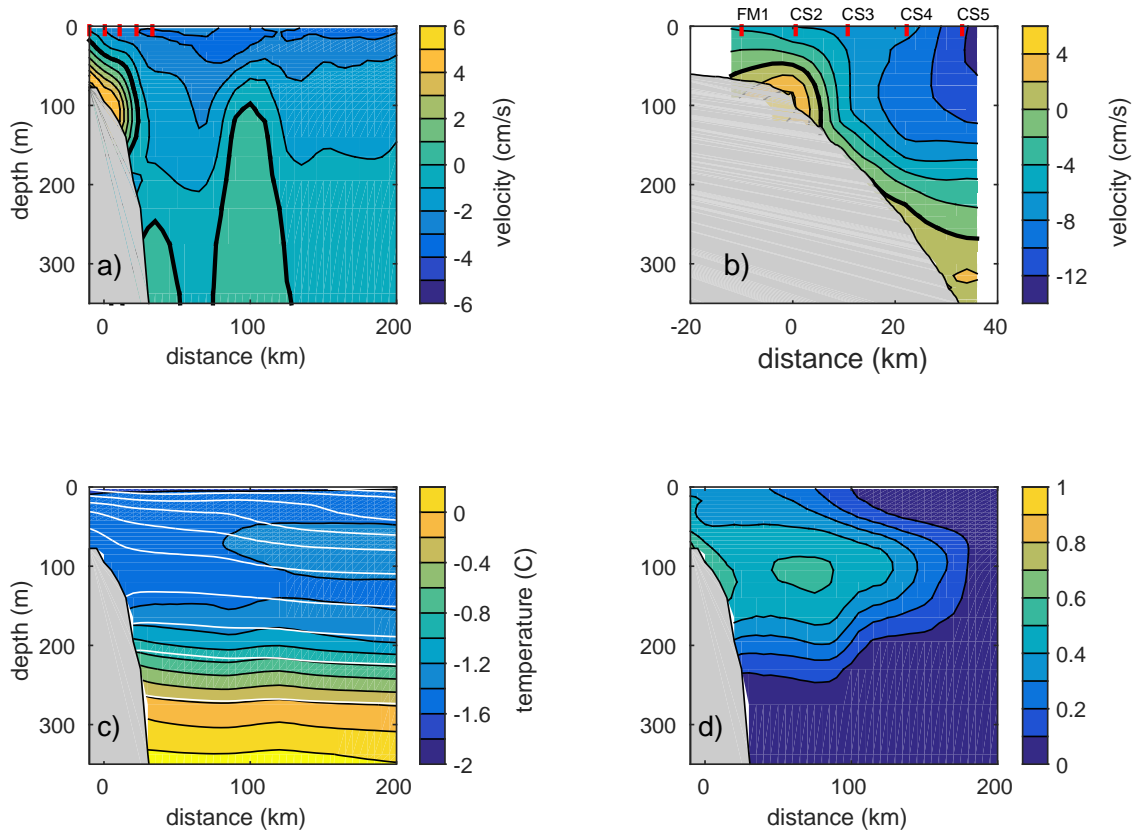
867 **Figure 4.** Mean transport streamfunction calculated down to 300 m depth over the two years
 868 of model integration (black contours). Bold contours mark the 0.5 and 1.0 Sv levels. White con-
 869 tours are the bottom topography down to 1000 m, contour interval is 20 m for depths less than
 870 100 m (thin lines) and 100 m between 100 and 1000 m (bold lines). The red lines indicate the
 871 locations of the sections shown in Figs. 5 and 6.



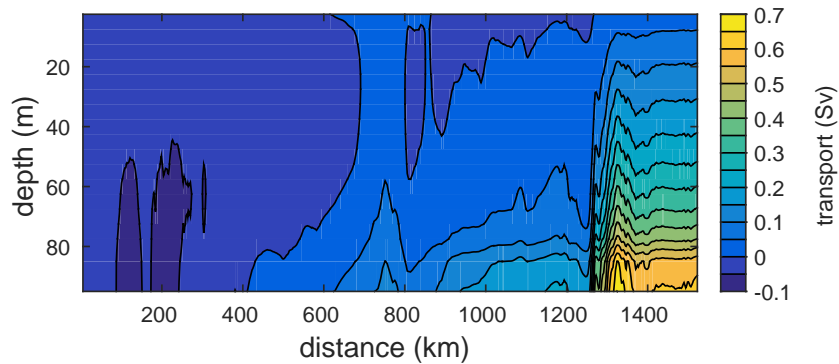
872 **Figure 5.** Section of the two year mean a) normal velocity and salinity (white contours, con-
 873 tour interval 0.5) from the model in Barrow Canyon (see location in Fig. 4). Positive velocities
 874 are down-canyon (to the northeast). The viewer is looking up-canyon (to the southwest). . b)
 875 Climatological mean along-canyon velocity and salinity (white contours, contour interval 0.5) at
 876 the mouth of Barrow Canyon measured by the JAMSTEC mooring array. The locations of the
 877 moorings are indicated by the red tick marks at the top of each figure.



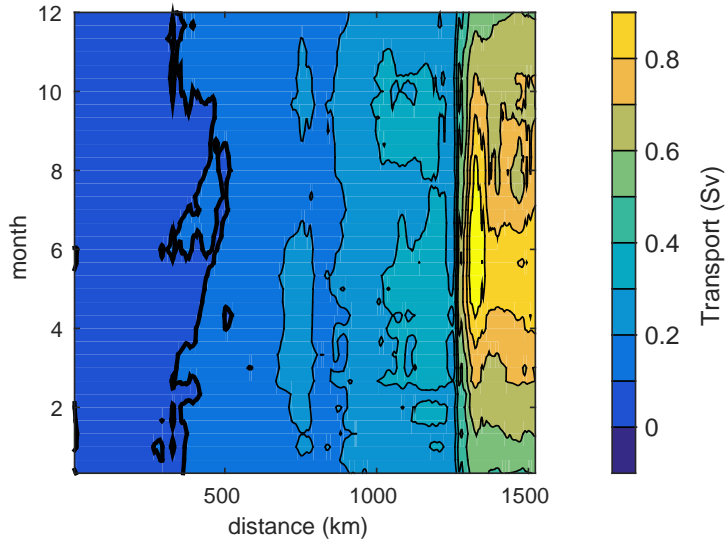
878 **Figure 6.** Section of the two year mean a) zonal velocity and salinity from the model at
 879 $x = 1000$ km (the approximate location of the mooring array). b) Year-long (2002-3) mean
 880 alongstream velocity and salinity near 152° W on the Beaufort slope (see Fig. 2 for the location of
 881 the array) from Nikolopoulos et al. (2009). Positive velocities are eastward. The locations of the
 882 moorings are indicated along the top by the red tick marks. The viewer is looking to the west.



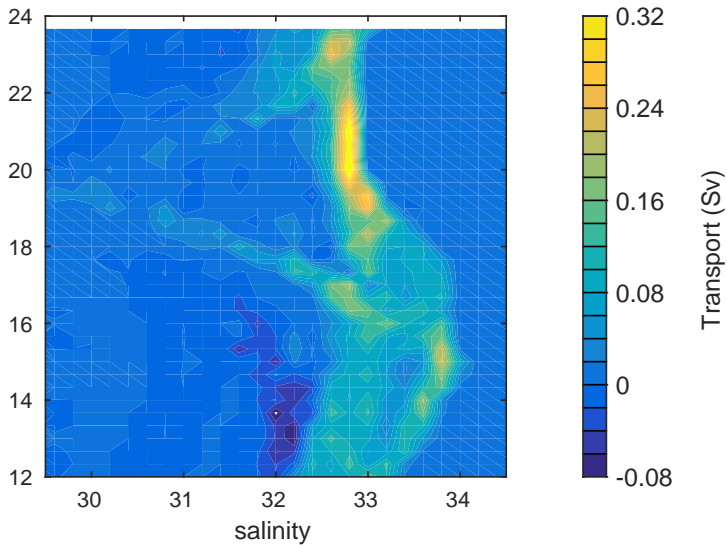
883 **Figure 7.** Mean sections between $x = 600$ km and $x = 830$ km for the final 6 months of
 884 a) along-topography velocity ($cm s^{-1}$); b) Year-long (2013-14) mean alongstream velocity near
 885 $157^{\circ}W$ on the Chukchi slope (see Fig. 2 for the location of the array) from *Li and Pickart* [2017].
 886 c) temperature (colors) and salinity (white contours, contour interval 0.5); d) Pacific water tracer.
 887 The offshore distance and along-topography velocity from the model are mapped relative to the
 888 75 m isobath. Positive velocities are eastward. The locations of the moorings are indicated along
 889 the top. The viewer is looking to the west.



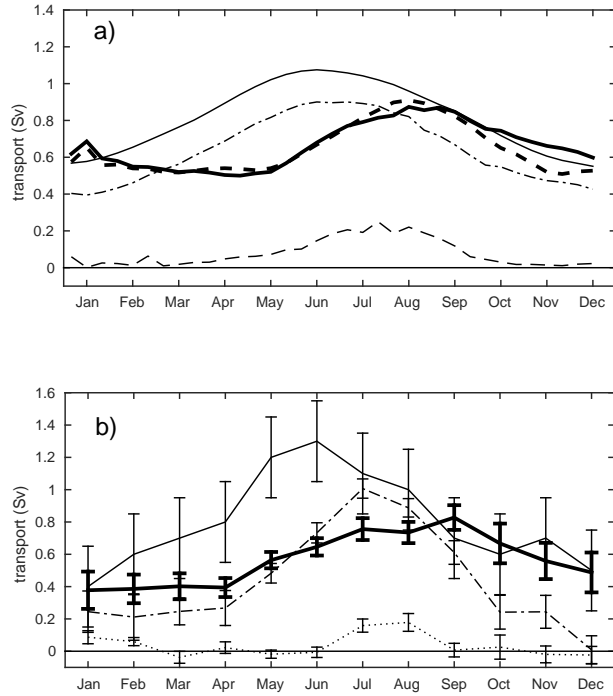
890 **Figure 8.** The transport across the 100 m isobath, integrated from surface to bottom and
 891 from the western boundary of the domain to $x = 1000$ km (Sv). This path is indicated on Fig. 3
 892 by the bold green line, with distance markers provided for reference.



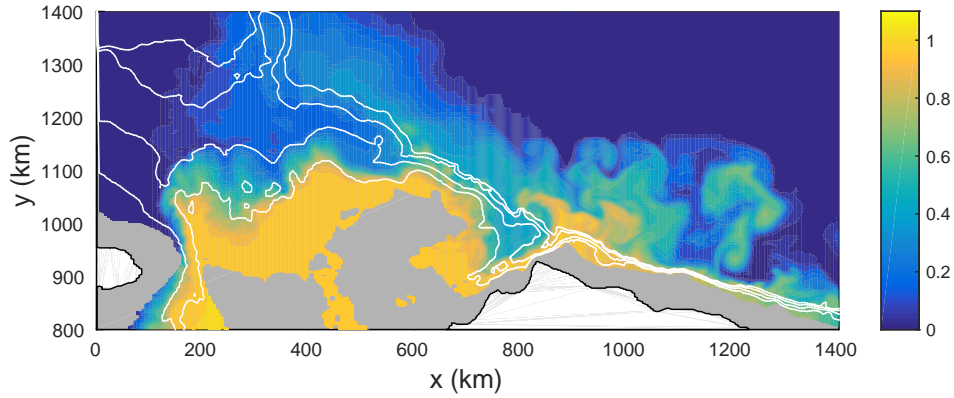
893 **Figure 9.** The transport across the 100 m isobath, integrated from surface to bottom as a
 894 function of distance from the western boundary of the domain and time. This is the average sea-
 895 sonal cycle based on two years of model integration. The 100 m isobath is indicated on Fig. 3 by
 896 the bold green line, with distance markers provided for reference.



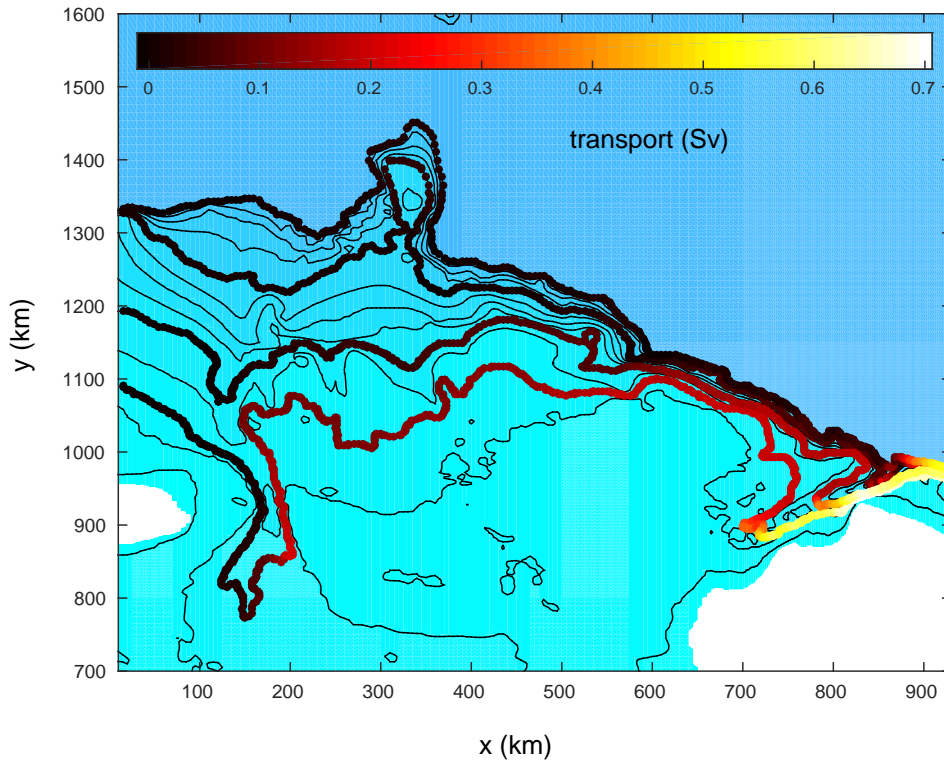
897 **Figure 10.** The transport across the 100 m isobath, between the model western boundary and
 898 $x = 1000$ km as a function of salinity (0.2 ppt increments) and time. This is calculated over the
 899 second year of integration only. The 100 m isobath is indicated on Fig. 3 by the bold green line.



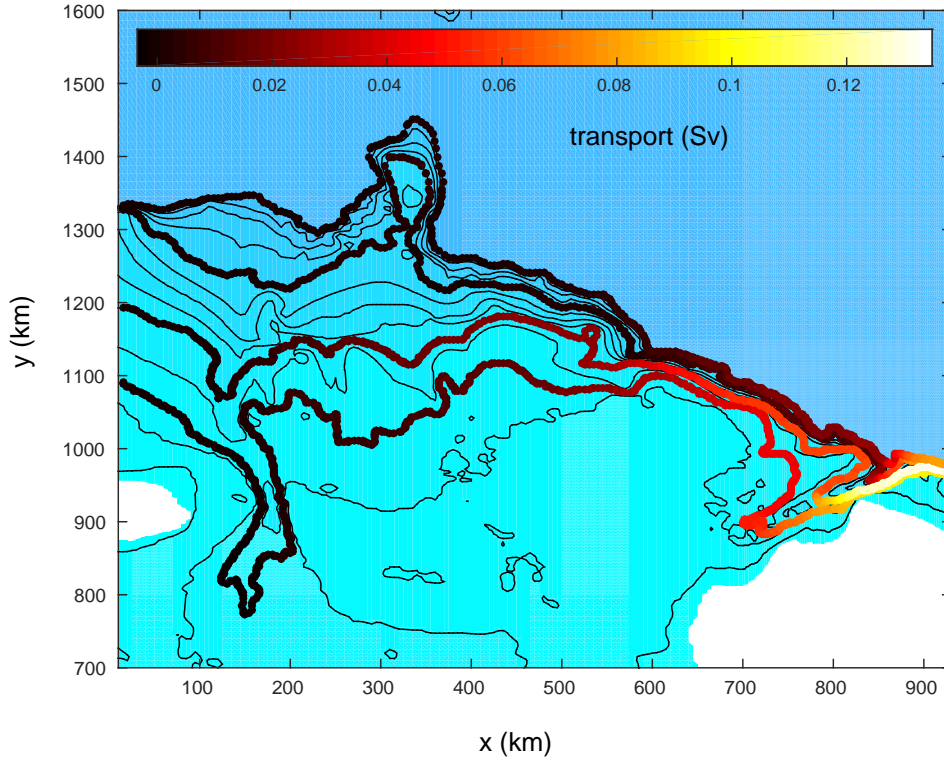
900 **Figure 11.** Seasonal mean timeseries of transports from a) the numerical model and b) moor-
 901 ing observations. Bold solid lines: a) westward transport between coast and $y = 1200$ km for
 902 the model (indicative of the Chukchi Slope Current) and b) based on the mooring array from
 903 2013-2014. The bold dashed line in a) is from the model runs with no seasonal cycle in Bering
 904 Strait velocity or wind and the full seasonal cycle in forcing of buoyancy at Bering Strait and
 905 surface heat flux. Thin solid lines: transport through Bering Strait (1990-2004 in b). Dot-dash
 906 lines: transport through Barrow Canyon (2000-2008; 2010-2016). Dashed line in a): difference in
 907 density between the surface and the bottom in Barrow Canyon for the full model run (kg m^{-3}).
 908 Dotted line in b): eastward transport in Beaufort shelfbreak jet (2008-2012).



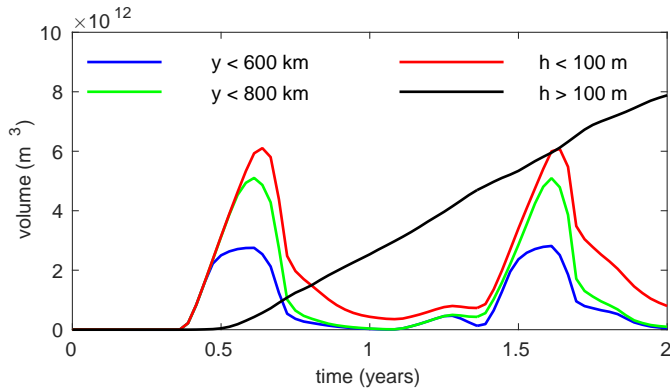
909 **Figure 12.** Pacific water tracer in the vicinity of the shelf break at 47.5 m depth at the end
 910 of year 2. The 60, 100, 200, and 300 m isobaths are indicated by the white contours. Topography
 911 shallower than 47.5 m is shaded gray, land is white.



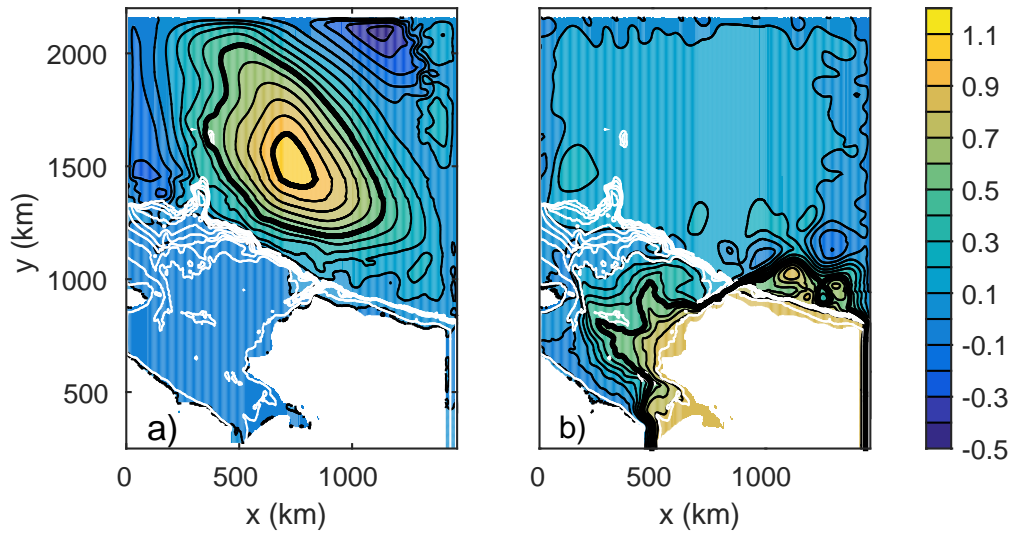
912 **Figure 13.** Cross-isobath transport (Sv) of Pacific water tracer along the 60, 100, 200, and
 913 300 m isobaths over the final year of integration. All start at zero at the western boundary and
 914 integrate eastward along the topographic contours. Positive values indicate transport towards
 915 deeper water.



916 **Figure 14.** Cross-isobath eddy transport (Sv) of Pacific water tracer along the 60, 100, 200,
 917 and 300 m isobaths over the final year of integration. All start at zero at the western bound-
 918 ary and integrate eastward along the topographic contours. Positive values indicate transport
 919 towards deeper water.



920 **Figure 15.** Volume of unventilated Pacific water within various regions of the Chukchi shelf
 921 and interior. Blue: south of $y = 600$ km. Green: south of $y = 800$ km. Red: shallower than 100
 922 m. Black: deeper than 100 m.



923 **Figure 16.** Mean upper ocean transport streamfunction (surface to 300 m) over the two year
 924 integrations for a) case with atmospheric forcing and a closed Bering Strait; b) forcing in Bering
 925 Strait but with no atmospheric forcing.